Special Section: Remote Sensing

Pardhasaradhi Teluguntla
Dongryeol Ryu*
Biju George
Jeffrey P. Walker

Multidecadal Trend of Basin-Scale Evapotranspiration Estimated Using AVHRR Data in the Krishna River Basin, India

Evapotranspiration (ET) is one of the most critical components of terrestrial water balance. Estimating reliable ET across a large region is, however, difficult due to the limited number of ground monitoring stations and the heterogeneous land surface conditions. In this work, spatially distributed monthly ET estimates in the Krishna River Basin, India, were derived using Advanced Very High Resolution Radiometer (AVHRR) data and the ground monitoring data sets from local meteorological stations for the 1983 to 2001 time period. A modified Penman–Monteith model with biome-specific canopy conductance was used to estimate the 8-km AVHRR ET. Ground validation was conducted using the lysimeter measurements and Landsat- and MODIS-based ET estimates from the same model aggregated to the AVHRR scale. The difference between the lysimeter measurements and 30-m Landsat estimates was only 5.3%, and the mean difference between the aggregated Landsat ET and the AVHRR ET estimates was <14%. The AVHRR ET estimates of this study showed that the basin-average ET increased continuously at the mean rate of 4.97 mm yr^{-1} yr^{-1} in the Krishna River Basin during 1983 to 2001. The subbasin-scale ET analyses showed an increasing trend of ET in the upstream subbasins, where irrigation development was active in the 1980s, compared with the other subbasins. Further sensitivity analyses based on land-use information showed that the increased ET in the basin is mainly due to the development of irrigation that occurred during the study period.

Abbreviations: AVHRR, Advanced Very High Resolution Radiometer; ET, evapotranspiration; fvc, fractional vegetation cover; GIMMS, Global Inventory Monitoring and Modeling Studies; MODIS, Moderate Resolution Imaging Spectroradiometer; NDVI, normalized difference vegetation index; NIR, near infrared; PM, Penman–Monteith; VPD, vapor pressure deficit.

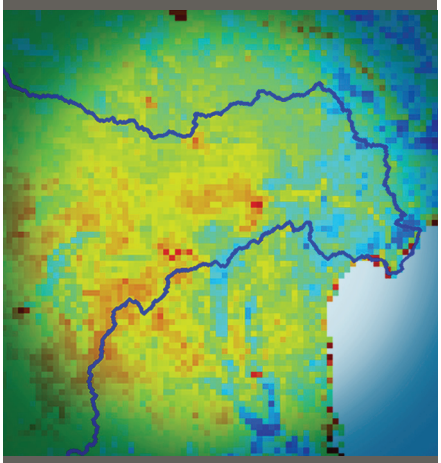

The AVHRR data were used to estimate evapotranspiration in the Krishna River Basin, India, for the period 1983 to 2001. Results show that the basin-average evapotranspiration (ET) increased continuously at the mean rate of 4.97 mm yr^{-1} yr^{-1} during this period. The land-use information showed that the increased ET was mainly due to the development of irrigation in the basin.

P. Teluguntla, D. Ryu, and B. George, Dep. of Infrastructure Engineering, Univ. of Melbourne, Parkville, 3010 VIC, Australia; and J.P. Walker, Dep. of Civil Engineering, Monash Univ., VIC 3800, Australia. *Corresponding author (dryu@unimelb.edu.au).

Vadose Zone J.
doi:10.2136/vzj2012.0118
Received 30 July 2012.

Evapotranspiration is one of the most critical processes of the water cycle, with significant spatial variability from point scale to river basin scale. Globally, about 62% of the precipitation that falls on land returns to the atmosphere via evapotranspiration (Jackson et al., 2001; Dingman, 2008), and of this land component, about 97% is evapotranspiration from land surfaces while 3% is open water evaporation. For arid and semiarid regions, ET comprises about 90% or more of the annual precipitation (Wilcox et al., 2003; Australian National Water Commission, 2007). Consequently, accurate estimation of ET plays an important role in water resource management.

There are a number of conventional methods available to estimate ET using surface meteorological observations. They are based on ground observations of air temperature, vegetation height, wind speed, relative humidity, and solar radiation. Such approaches, however, are typically point measurements, covering only a small portion of the land surface. Limitations to measuring ET at large scales using ground-based methods can be overcome in part by using remotely sensed imagery of land surface parameters such as vegetation indices and the land surface temperature (Bastiaanssen et al., 1998a; Kustas et al., 2003; Tasumi et al., 2005; Allen et al., 2007b). Spatially distributed land surface parameters from remote sensing techniques can be combined with field measurements to fully capture the spatial trends among various land use types due to spatial heterogeneity at regional scales (Gowda et al., 2008). Satellite-based ET algorithms based on a surface energy balance (SEB), such as the Surface Energy Balance Algorithm for Land (SEBAL) (Bastiaanssen et al., 1998a, 1998b), the Surface Energy Balance System (SEBS) (Su, 2002), Mapping Evapotranspiration with Internalized Calibration (METRIC) (Tasumi et al., 2005; Allen et al., 2007a, 2007b), are now frequently applied to produce ET estimates for water resources management. Landsat imagery is commonly used to

produce high-resolution ET estimates at the field scale due to the thermal band available at 60-m resolution. The SEB models require uniformly dry and wet pixels within the scene, which makes the use of medium- to high-resolution thermal infrared (TIR) data necessary to provide reliable ET estimates. For coarse-resolution imagery, however, sampling uniformly wet and dry patches of land, where the latent heat flux is assumed to be maximum and zero, respectively, is very difficult. A drawback of using the Landsat or other high-resolution satellite images is that their infrequent image acquisition (due to the narrow field of view) makes the concurrent estimation of ET difficult at large scales. Another limitation is that algorithms based on the use of near infrared (NIR) and TIR wavelengths are sensitive to the effects of clouds and cloud shadows. As a result, there may be only a few images with a sufficient cloud-free coverage suitable for processing (Kalma et al., 2008; Allen et al., 2007a). Therefore, analysis of seasonal fluctuations of ET at large scales using SEB models may not be feasible.

In recent years, studies have estimated ET from regional to global scales using process-based models and input data from remote sensing, eddy covariance flux towers, and reanalyses (Cleugh et al., 2007; Mu et al., 2007; Leuning et al., 2008; Zhang et al., 2009; Ferguson et al., 2010; Vinukollu et al., 2011b). A simple resistance algorithm based on the leaf area index and other empirically derived parameters were combined with the Penman–Monteith (PM) model. For example, Zhang et al. (2010) used spatially distributed ET estimates from a modified PM model with biome-specific conductance parameterized by the normalized difference vegetation index (NDVI) to analyze a basin-scale water balance. In this research, we applied the modified PM model in the Krishna River Basin, India, to estimate basin-scale ET from 1983 to 2001. During this period, significant changes in land use and river discharge occurred in the basin (Bouwer et al., 2006; Biggs et al., 2007).

The Krishna River Basin in India has experienced significant changes in the basin-scale water balance in recent decades. For example, the river discharge from the basin declined from 830 m^3 s^{-1} in the 1970s to almost nothing in 2002 without significant changes in annual rainfall (Bouwer et al., 2006; Biggs et al., 2007; Venot et al., 2007). The observed changes in the water balance of the catchment have been attributed to the development of water storage for agricultural, industrial, and urban water consumption (Bouwer et al., 2006; Van Rooijen et al., 2010). Hydrologic structures such as dams and reservoirs are known to change the temporal patterns of the hydrologic cycle (Haddeland et al., 2006); however, the impact of altered water use on the spatiotemporal changes in ET in the basin has not yet been examined. While there exist long-term ET estimates based on land surface models, such as the Global Land Data Assimilation System, available at 1° resolution (http://disc.sci.gsfc.nasa.gov/hydrology), they do not extend back to the predevelopment periods of the Krishna River Basin (1970s–1980s). Also, they have not been validated in this area using local ground observations and are unable to account for the effects of irrigation. Alternatively, the MOD16 product derived from Moderate Resolution Imaging Spectroradiometer (MODIS) data provides ET estimates at 5-km spatial resolution; however, the ET product is available only from 2001 onward. On the other hand, global coverage of surface parameters (8-km resolution) from NOAA's AVHRR Pathfinder provide a great opportunity to monitor changes in vegetation density (Thenkabail et al., 2009) and other land surface properties with time since 1983. Although higher spatial resolution data are preferable for ET estimation, they were not used in this study due to the inadequate temporal resolution (Landsat) and availability (MODIS), as mentioned above. Consequently, we estimated ET in this study by combining 8-km AVHRR imagery and ground-based metrological data, using the modified Penman–Monteith model with biome-specific canopy conductance determined by NDVI (Zhang et al., 2010). Fortnightly composites of 8-km NDVI from the Global Inventory Monitoring and Modeling Studies (GIMMS) at NASA were used based on AVHRR measurements from 1983 to 2001.

Study Area and Data Sets

Study Area

The Krishna River Basin, located in southern India, lies between 73°15′ to 81°20′ E and 13°5′ to 19°20′ N (Fig. 1) with a total basin area of 258,912 km^2. It is a multistate basin encompassing the Indian states of Karnataka (KAR), Maharashtra (MH), and Andhra Pradesh (AP) and is one of India's largest domestic waterways, supplying water to 80 million people.

The river originates in the Western Ghats at an elevation of about 1337 m, just north of a town called Mahabaleshwar at about 64 km from the Arabian Sea, and flows for about 1400 km before reaching the Bay of Bengal. The principal tributaries joining the Krishna River are the Ghataprabha, Malaprabha, Bhima, Tungabhadra, Vedavathi, and Musi. The basin is relatively flat, except for the Western Ghats and some forested hills in the center and northeast. The average annual rainfall is 850 mm (spatially varying 500–2000 mm); the maximum temperature varies between 20 and 42°C and the minimum temperature between 8 and 30°C. There are two major cropping seasons: Kharif occurs from June to November and Rabi from December to March in the following year (George et al., 2011). The monsoon starts in June and lasts until October. The Kharif rainfed crops depend completely on the monsoon, and any changes in its timing or intensity affect the crop yield. Crops grown in the service area of a dam or reservoir depend on both rainfall and irrigation. The scheduling of irrigation in the service area depends on the amount of rainfall.

Average annual discharge to the ocean was 57 km^3 (29% of rainfall) before the 1970s (pre-irrigation period) at Vijayawada, which is the last measuring point in the basin, located 105 km upstream of the river's outlet to the ocean (Biggs et al., 2007). Construction of dams and irrigation expansion continued

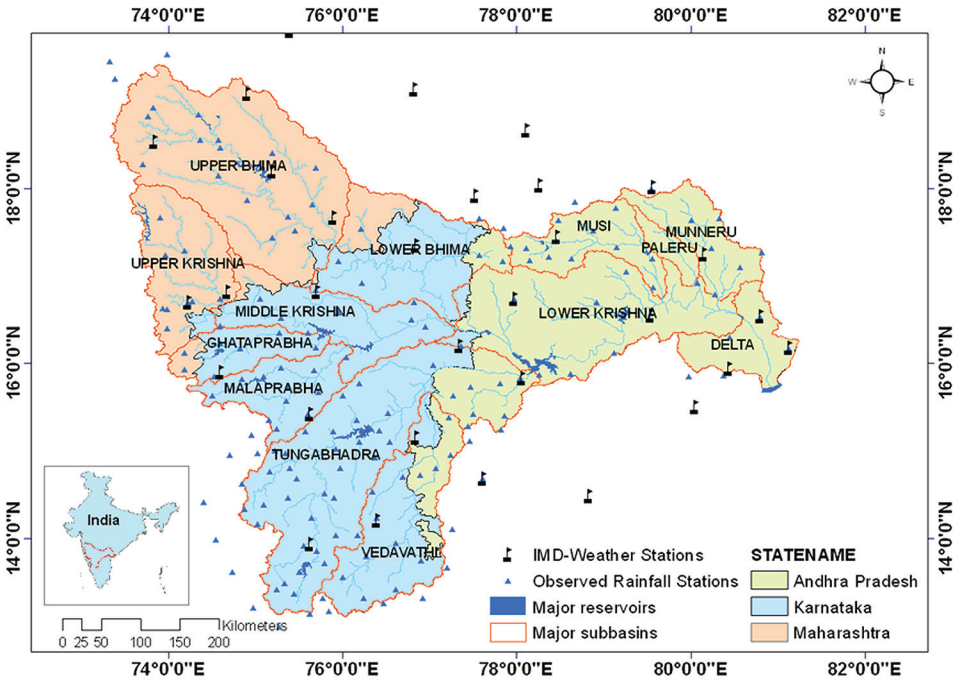

Fig. 1. Location map of the Krishna River Basin with state names and boundaries, river network, major surface water reservoirs, meteorological station network monitored by the Indian Meteorological Department (IMD), and additional rainfall observation stations.

rapidly throughout the '70s and '80s, resulting in a decrease in the annual average discharge to <13 km^3 (nearly 7% of rainfall) in the '90s. This reduced discharge has continued to present times with no significant decrease in rainfall. The current average annual discharge is only 22% of the pre-irrigation period discharge to the ocean; as a consequence, it is assumed that the discharge deficit is consumed by crops to meet the ET demand.

Meteorological Data

There are various sources of data available for inputs to the ET retrieval models. They include surface meteorological variables and vegetation parameters from long-term monitoring stations and remotely sensed products. In the Krishna River Basin, a network of meteorological stations (Fig. 1) are maintained by the Indian Meteorological Department (IMD), with further meteorological stations maintained by other research institutions including ICRISAT, the Central Research Institute for Dryland Agriculture (CRIDA), and different state government departments. Data on minimum air temperature, maximum air temperature, wind speed, relative humidity and the duration of sunshine hours recorded by the weather stations were collected for the study period 1983 to 2001. Rainfall data were obtained from 178 rain gauge stations maintained by various departments in and around the study area. Hydrologic data such as observed discharge and reservoir storage capacity were collected from the Central Water Commission, Department of Water Resources of India.

Spatially interpolated meteorological variables required for the ET model, such as minimum air temperature, maximum air temperature, wind speed, relative humidity, and duration of sunshine hours, were generated from the available station data using the inverse distance weight interpolation method. The actual evapotranspiration (ET_a) for field-scale validation was measured by the weighing lysimeters at the Hyderabad station (17°31′2″ N, 78°16′33″ E) within the Krishna River Basin, which is maintained by the IMD. Lysimeter data were obtained from 1987 to 1998 for Hyderabad (ICRISAT). The average daily ET_a and other information available from IMD were collected and used to validate field-scale (30-m resolution) Landsat ET estimates derived using the method described below. The 30-m-resolution Landsat ET estimates were later coarsened to 8-km resolution to validate the AVHRR-derived ET estimates.

Satellite Data

Global semimonthly composites of the NDVI, called the AVHRR GIMMS NDVI (Tucker et al., 2005), were used in this study to calculate the basin-scale monthly ET maps of the Krishna River Basin from 1983 to 2001. This data set is available at the Global Land Cover Facility of the University of Maryland (http://glcf.umd.edu/data/gimms/). The NDVI was estimated from NIR (Band 2) and red (Band 1) bands of AVHRR by

$$\mathrm{NDVI} = \frac{\mathrm{NIR} - \mathrm{RED}}{\mathrm{NIR} + \mathrm{RED}} \quad [1]$$

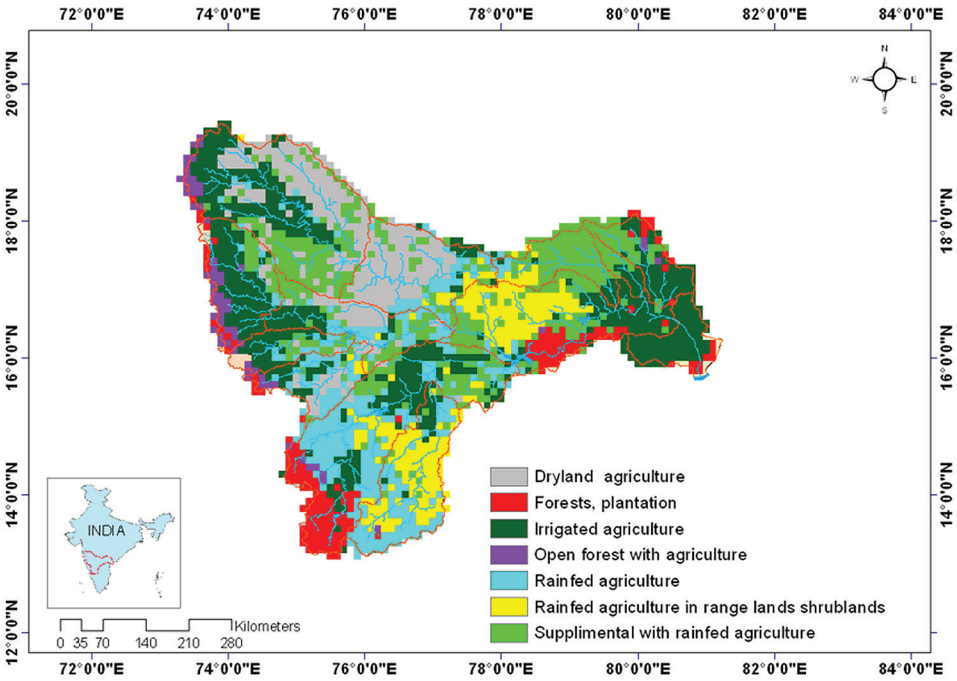

Fig. 2. Land use–land cover map of the Krishna River Basin derived from 8-km AVHRR data (methodology developed by Thenkabail et al., 2007).

The daily albedo data for the AVHRR ET estimates during the whole study period were derived from the NASA World Climate Research Program/Global Energy and Water Cycle Experiment's Surface Radiation Budget Release 3.0 data sets (Pinker and Laszlo, 1992), which were resampled at 8-km AVHRR GIMMS resolution. Due to the large discrepancy of the scales between the AVHRR imagery and the lysimeter measurements, high- and medium-resolution images from Landsat and MODIS were used to validate the ET algorithm adopted in this study. Cloud-free images of Landsat-5 and Landsat-7 that included the Hyderabad lysimeter station (Path = 144, Row = 048) for the years 1998 (6 May and 7 June) and 2000 (1 March and 29 December) were used to estimate field-scale ET values (30-m resolution), which were compared with the lysimeter measurements. The selected imagery is predominantly over a subcatchment of the study area (Fig. 1) called the Musi catchment. Bands 3 (red) and 4 (NIR) of the Landsat images were used to estimate the NDVI and the other visible bands to calculate the albedo at 30-m resolution.

The MODIS-Terra data for the same area as the Landsat images were obtained from calibrated global continuous time-series data sets distributed by NASA's Land Processes Distributed Active Archive Center (http://www.usgs.gov/science/cite-view.php?cite=401). Bands 1 (red) and 2 (NIR) of the MODIS (June 2000–May 2001) 8-d composites (MOD09Q1) were used to calculate the NDVI. Surface albedo was calculated by equal weighting of the reflectance in NIR and red bands. Land use and land cover (LULC) information is an important input to the modified PM model based ET estimation. We used the methodology developed by Thenkabail et al. (2007) to prepare land cover maps in this study. Annual time series of the LULC map, which is composed of seven different land cover classes (Fig. 2), was derived from the AVHRR images for the study area and used for the ET retrieval.

Description of Methodology

Evapotranspiration Algorithm

There are several approaches to calculating ET using remotely sensed surface variables, including surface energy based algorithms and physically based algorithms. The PM model (Monteith, 1965) is arguably the most popular model to calculate evaporation in hydrologic applications. Based on the PM equation, Priestley and Taylor (1972) defined equilibrium ET over large regions by replacing surface and aerodynamic resistance terms with an empirical multiplier. While the PM equation is more theoretically correct, the Priestley and Taylor (PT) model is simpler than the PM model, thus requiring simpler parameterization and inputs. Both methods have been applied to estimate ET over large regions by incorporating satellite imagery (Cleugh et al., 2007; Mu et al., 2007; Fisher et al., 2008; Vinukollu et al., 2011a). In this study, a modified PM equation was applied with AVHRR NDVI-based vegetation attributes and daily surface meteorological data from weather stations to calculate ET from the land surface. Open-water evaporation from the reservoirs in the basin was estimated using the PT model.

An NDVI-based ET algorithm developed by Zhang et al. (2009) was used in this study to derive biome-specific canopy conductance

as a function of the NDVI for the biome types in the Krishna River Basin. In the algorithm, the open-water pixels were identified from the remotely sensed imagery first, and a separate scheme based on the PT model was used to estimate the ET from open water. For vegetated pixels, ET was partitioned into soil evaporation and canopy transpiration by partitioning the available energy for bare soil evaporation and transpiration, respectively, using the fractional vegetation cover. The fractional vegetation cover (fvc) is defined as the fraction of ground surface covered by the maximum extent of vegetation canopy (varying between 0 and 1) as follows:

$$\mathrm{fvc}=\frac{\mathrm{NDVI}-\mathrm{NDVI}_{\min}}{\mathrm{NDVI}_{\max}-\mathrm{NDVI}_{\min}} \quad [2]$$

where $\mathrm{NDVI}_{\max}$ and $\mathrm{NDVI}_{\min}$ are the maximum and the minimum NDVIs within the entire study areas, which are assumed to represent the vegetation density of densely vegetated areas and bare soil, respectively. The NDVI varies between −1 and 1, with a relatively strong sensitivity to the biomass of the vegetation canopy. Densely vegetated areas have high NDVI while bare soils have lower but positive NDVI values.

In the NDVI-based ET algorithm, energy at the land surface is governed by the surface energy balance equation:

$$R_n = H + \lambda E + G \quad [3]$$

where R_n is the net radiation at the surface, H is the sensible heat flux, λE is the surface latent heat flux, and G is the soil heat flux. The value of R_n is calculated as

$$R_n = R_{ns} - R_{nl} = (1-\alpha)R_{sin} - R_{nl} \quad [4]$$

where R_{ns} is the net shortwave radiation, R_{sin} is the incoming shortwave radiation, α is the surface albedo, and R_{nl} is the outgoing net longwave radiation, which is calculated by the FAO-56 method (Allen et al., 1998):

$$R_{nl} = \sigma\left(\frac{T_{\max,K}^4 + T_{\min,K}^4}{2}\right)\left(0.34 - 014\sqrt{e_a}\right) \times\left(1.35\frac{R_{sin}}{R_{so}} - 0.35\right) \quad [5]$$

where σ is the Stefan–Boltzmann constant, $T_{\max.K}$ and $T_{\min,K}$ are the mean daily maximum and minimum air temperatures, respectively, in Kelvin, e_a is the actual daily air water vapor pressure, and R_{so} is the clear-sky incoming shortwave radiation.

The ET for vegetated areas was partitioned into soil evaporation and canopy transpiration by partitioning the available energy (A) for ET (Mu et al., 2007) using the fvc derived from the NDVI. The available energy for ET is determined as the difference between net radiation (R_n) and soil heat flux (G), with R_n calculated based on the FAO-56 method (Allen et al., 1998). The value of G is calculated as

$$G = R_n\left[\Gamma_c + (1-\mathrm{fvc})(\Gamma_s - \Gamma_c)\right] \quad [6]$$

where Γ_c and Γ_s are the ratios of soil heat flux to net radiation for a fully vegetated surface (Γ_c = 0.05) and bare soil (Γ_s = 0.315) (Su,2002).

The available energy (A) is linearly partitioned into energy components for the canopy and soil surface using the fvc (Mu et al., 2007) such that

$$A_{\mathrm{canopy}} = A(\mathrm{fvc}) \quad [7]$$

$$A_{\mathrm{soil}} = A(1-\mathrm{fvc}) \quad [8]$$

The PM equation is used to calculate vegetation transpiration:

$$\lambda E_{\mathrm{canopy}} = \frac{\Delta A_{\mathrm{canopy}} + \rho C_p (e_{sat} - e_a) g_a}{\Delta + \gamma(1 + g_a/g_c)} \quad [9]$$

where $\lambda E_{\mathrm{canopy}}$ is the latent heat flux of the canopy, λ is the latent heat of vaporization, $\Delta = \mathrm{d}e_{sat}/\mathrm{d}T$ is the slope of the curve relating the saturated water vapor pressure (e_{sat}) to the air temperature (T), $e_{sat} - e_a$ is the vapor pressure deficit (VPD), ρ (kg m^{-3}) is the air density, C_p (J kg^{-1} K^{-1}) the specific heat capacity of air, and g_a (m s^{-1}) is the aerodynamic conductance calculated according to PM model. The psychrometric constant γ is given by

$$\gamma = \frac{M_a}{M_w}\frac{C_p P_{air}}{\lambda} \quad [10]$$

where M_a (kg mol^{-1}) and M_w (kg mol^{-1}) are the molecular masses of dry and wet air, respectively, P_{air} (Pa) is the air pressure, and g_c is the canopy conductance, which is calculated using the Jarvis–Stewart type canopy conductance model (Zhang et al., 2009):

$$g_c = g_0(\mathrm{NDVI}) \times m(T_{\mathrm{day}}) \times m(\mathrm{VPD}) \quad [11]$$

where g_0(NDVI) is the biome-dependent potential (i.e., maximum) value of g_c, which is a function of NDVI, T_{day} (°C) is the daylight

average air temperature, $m(T_{day})$ is a moisture stress factor as a function of T_{day}, and $m(\mathrm{VPD})$ is a moisture stress factor as a function of the VPD. The temperature stress factor $m(T_{day})$ follows the equation developed by June et al. (2004) with an optimum temperature T_{opt}:

$$m(T_{day}) = \begin{cases} 0.01 & T_{day} \le T_{close\text{-}min} \\ \exp\left[-\dfrac{(T_{day}-T_{opt})^2}{\beta}\right] & T_{close\text{-}min} < T_{day} < T_{close\text{-}max} \\ 0.01 & T_{day} \ge T_{close\text{-}max} \end{cases} \quad [12]$$

where T_{opt} (°C) is the biome-specific optimal air temperature for photosynthesis, $T_{close\text{-}min}$ (°C) and $T_{close\text{-}max}$ (°C) are the biome-specific minimum and maximum critical temperatures for stomatal closure and the effective cessation of plant photosynthesis, β (°C) a biome-specific parameter that is the difference in temperature from T_{opt} at which temperature stress factors fall to 0.37 (i.e., e^{-1}). The term $m(\mathrm{VPD})$ is calculated as

$$m(\mathrm{VPD}) = \begin{cases} 1.0 & \mathrm{VPD} \le \mathrm{VPD}_{open} \\ \dfrac{\mathrm{VPD}_{close}-\mathrm{VPD}}{\mathrm{VPD}_{close}-\mathrm{VPD}_{open}} & \mathrm{VPD}_{open} < \mathrm{VPD} < \mathrm{VPD}_{close} \\ 0.1 & \mathrm{VPD} \ge \mathrm{VPD}_{close} \end{cases} \quad [13]$$

where VPD_{open} is the biome-specific critical value of VPD at which the canopy stomata are completely open and VPD_{close} is the biome-specific critical value of VPD at which the canopy stomata are completely closed.

Soil evaporation was calculated using the soil evaporation equation from Mu et al. (2007) and Zhang et al. (2010), which is a combination of the adjusted PM equation and a complementary relationship suggested by Bouchet (1963). The soil evaporation equation and its auxiliary equations include:

$$\lambda E_{Soil\text{-}pot} = \frac{\Delta A_{Soil} + \rho C_p \mathrm{VPD} g_a}{\Delta + \gamma(g_a/g_{totc})} \quad [14]$$

$$\lambda E_{Soil} = \lambda E_{Soil-pot}\left(\frac{\mathrm{RH}}{10}\right)^{\mathrm{VPD}/k} \quad [15]$$

$$g_a = g_{ch} + g_{rh} \quad [16]$$

$$g_{rh} = \frac{4.0\sigma T_{day}^3}{\rho C_p} \quad [17]$$

$$g_{totc} = g_{tot} + G_{corr} \quad [18]$$

$$G_{corr} = \left(\frac{273.15+T_{day}}{293.15}\right)\frac{101{,}300}{P_{air}} \quad [19]$$

where RH is the relative humidity (%); $(\mathrm{RH}/100)^{\mathrm{VPD}/k}$ is a moisture constraint on soil evaporation, which is an index of the soil water deficit based on the complementary relationship whereby surface moisture status is linked to and reflects the evaporative demand of the atmosphere based on the assumption that the soil moisture is reflected in the adjacent atmospheric moisture; k (Pa) is a parameter to fit the complementary relationship that reflects the relative sensitivity to VPD and is adjusted for different vegetation types; g_{rh} (m s^{-1}) is the conductance to radiative heat transfer calculated using Eq. [17]; g_{ch} (m s^{-1}) is the conductance to convective heat transfer under the boundary layer conditions and the assigned g_{ch} is a biome-specific constant (see Table 1); g_{tot} (m s^{-1}) is the total aerodynamic conductance to vapor transport and the combination of surface and aerodynamic conductance components; g_{totc} (m s^{-1}) is the value of g_{tot} corrected for standard temperature and pressure using a correction coefficient (G_{corr}), and g_{tot} is adjusted by land cover type. Potential surface conductance (g_0) for each biome type is derived using the NDVI as

$$g_0(\mathrm{NDVI}) = \frac{1}{b_1 + b_2\exp(-b_3\mathrm{NDVI})} + b_4 \quad [20]$$

where b_1 (s m^{-1}), b_2 (s m^{-1}), b_3 (dimensionless), and b_4 (s m^{-1}) are the observed parameters (see Table 1) from Mu et al. (2007) and Zhang et al. (2009). Considering $g_0(0) = 0$, b_4 is equal to $-1/(b_1 + b_2)$.

Validation

Typical ground-based measurement systems for ET validation include lysimeters and in situ meteorological techniques such as the eddy covariance (EC) flux (Paco et al., 2006) and the Bowen ratio methods (Drexler et al., 2004). Unfortunately, neither the EC flux station nor the Bowen ratio system is available in and around the study area to validate the ET product. Thus field-level ET_a measured by weighing lysimeter at the Hyderabad lysimeter experiment station located in the crop field (17°31′2″ N, 78°16′33″ E) was used to validate the remotely sensed ET products. A weighing lysimeter is the standard instrument for measuring actual crop water use under various field conditions and for measuring changes in soil moisture during the cropping season. Weighing lysimeters are also often used

Table 1. The biome properties used for the AVHRR normalized difference vegetation index (NDVI)-based evapotranspiration algorithm in the Krishna River Basin. Values were obtained from Zhang et al. (2010).

Parameter	Cropland	Grassland	Mixed forest	Shrubland
Min. optimal air temperature for stomata closure ($T_{close\text{-}min}$), °C	−8	−8	−7	−8
Max. optimal air temperature for stomata closure ($T_{open\text{-}max}$), °C	45	40	45	40
Critical vapor pressure deficit at which stomata are closed (VPD_{close}), Pa	3800	3900	2800	3700
Critical vapor pressure deficit at which stomata are open (VPD_{open}), Pa	650	650	650	500
Optimal air temperature for photosynthesis (T_{opt}), °C	20	20	25	10
Difference from T_{opt} at which temperature stress factors fall to 0.37 (β), °C	30	30	25	30
Fitting parameter k, Pa	450	500	200	50
Total aerodynamic conductance to vapor transport (g_{tot}), m s^{-1}	0.003	0.001	0.002	0.012
Conductance to convective heat transfer (g_{ch}), m s^{-1}	0.04	0.04	0.01	0.04
Parameter b_1, s m^{-1}	105	175	85.8	179
Parameter b_2, s m^{-1}	300	2000	695	179
Parameter b_3	3	6	4	8

to calibrate and validate other methods for estimating ET_a (Mohan and Arumugam, 1994; Tyagi et al., 2000; DehghaniSanij et al., 2004; Biggs et al., 2008).

Comparison between satellite-retrieved latent heat flux and ground-based measurements, however, raises several issues. Two of the main issues are the difference in spatial scales between the satellite retrievals and the ground measurements, and the heterogeneity of the land surface parameters within the satellite footprints (Kustas et al., 2004; Li et al., 2008). Validation of coarse-resolution ET data over a large region has been a typical challenge (Kalma et al., 2008), with no robust methods or data sets existing at regional scales. Field measurements from experimental sites cannot be directly compared with the corresponding 8-km ET estimates due to the sub-pixel-scale surface heterogeneity (Kalma et al., 2008).

To validate coarse-resolution (8-km) ET estimates using the point-scale lysimeter measurements, we first validated ET estimates from a high-resolution satellite, Landsat, over the lysimeter station. We assumed that the high-resolution ET estimates from Landsat can reproduce the variability of ET caused by the spatial heterogeneity of land surface features. Consequently, by validating a small subset of the Landsat ET using the lysimeter measurements, coarser resolution ET from MODIS and AVHRR can then be validated using the upscaled Landsat estimates. Likewise, upscaled MODIS ET estimates were used to validate the 8-km AVHRR ET estimates. The modified PM model, described above, was applied to cloud-free images of Landsat data collected on 6 May and 7 June 1998. The high-resolution (30-m) ET estimates validated with the lysimeter measurements were then aggregated to the coarse resolution (8 km) for comparison. In addition, due to the lack of cloud-free Landsat images during the period of lysimeter measurements and the limited size of the Landsat scene compared with the study area, the medium-resolution (250-m) ET estimates from MODIS were also compared with the AVHRR-derived ET. The Landsat ET was aggregated to 250-m resolution and compared with the MODIS estimates. Both Landsat- and MODIS-derived ET estimates were then aggregated to 8-km resolution to compare with the AVHRR data.

Results and Discussion

Monthly actual evapotranspiration was estimated using AVHRR-GIMMS satellite images and daily meteorological data for the period 1983 to 2001 with the modified PM equation in two separate components, vegetation transpiration and soil evaporation. First, high- to medium-resolution ET estimates (Landsat and MODIS) were validated against ground-based ET measurements at a lysimeter station. Then spatial and temporal patterns of ET in the Krishna River Basin were developed, and finally the impact of land cover types and irrigation development on the observed ET patterns was investigated.

Validation of Evapotranspiration

As described above, ET was estimated from high-resolution (30-m) Landsat data across the lysimeter experiment area for overpasses on 6 May and 7 June 1998. These ET estimates were compared with field-level ET_a data measured using a weighing lysimeter. The difference between the Landsat and lysimeter ET values was estimated as 0.15 mm d^{-1} in May 1998 and 0.01 mm d^{-1} in June 1998 (see Table 2). The 30-m Landsat ET value is smaller than the lysimeter measurements by 0.08 mm d^{-1} (5.3%) on average.

The consistency between daily ET estimates from 30-m Landsat and 250-m MODIS data was compared for March and December 2000 by coarsening the Landsat ET to the MODIS resolution. The Landsat ET map was aggregated to the 250-m MODIS resolution, using a simple averaging technique, taking the Landsat 30-m pixels

Table 2. Comparison of the evapotranspiration (ET) values determined by lysimeter, Landsat, MODIS, and AVHRR at various spatial scales in the Musi catchment region.

Sensor	Scale	Evapotranspiration			
		May 1998	June 1998	March 2000	December 2000
		mm d^{-1}			
Lysimeter	30 m	1.50	1.50		
Landsat		1.35	1.49		
Landsat	250 m			1.33	1.76
MODIS				1.42	1.61
Landsat	8 km			1.36	1.78
MODIS				1.43	1.63
AVHRR†				1.21	1.56
AVHRR-UMT‡				0.17	1.20

† ET estimates of this study.
‡ ET estimates of Zhang et al. (2010).

Table 3. Comparison between 8-km AVHRR mean evapotranspiration (ET) and aggregated 8-km MODIS mean ET over the Musi subbasin (June 2000–May 2001).

Month and year	AVHRR mean ET†	MODIS mean ET‡	Correlation (r)	RMSD
	mm d^{-1}			mm d^{-1}
June 2000	1.93	2.00	0.56	0.16
July 2000	2.19	2.30	0.59	0.16
Aug. 2000	2.28	1.75	0.36	0.28
Sept. 2000	2.90	2.90	0.75	0.17
Oct. 2000	2.56	2.57	0.81	0.19
Nov. 2000	2.21	2.00	0.64	0.19
Dec. 2000	1.78	1.62	0.75	0.14
Jan. 2001	1.65	1.50	0.81	0.13
Feb. 2001	1.66	1.44	0.89	0.16
Mar. 2001	1.63	1.42	0.89	0.14
Apr. 2001	1.30	1.15	0.78	0.13
May 2001	0.78	0.69	0.75	0.09

† AVHRR mean ET was calculated by averaging the 8-km AVHRR ET values of all pixels in the catchment.
‡ MODIS mean ET was calculated by averaging the aggregated 8-km MODIS ET of all pixels in the catchment.

that fell in the grid cell of a MODIS pixel. The comparison of aggregated Landsat ET with the corresponding MODIS ET over a 50- by 50-km region in the Musi catchment resulted in a root mean square difference (RMSD) of 0.165 mm d^{-1}. Lastly, the 30-m Landsat ET and 250-m MODIS ET estimates were aggregated to 8-km AVHRR-GIMMS resolution using the simple averaging technique used for Landsat-MODIS comparison. The ET estimates from three sensors at 8-km-resolution pixels that included the lysimeter experiment site were compared for two monthly ET maps (March and December 2000). Daily meteorological data were used to calculate daily Landsat 30-m ET, and the NDVI was assumed to be constant throughout the month; subsequently, monthly ET maps were prepared by averaging the daily ET estimates. The AVHRR ET estimates were low in comparison to Landsat and MODIS estimates by 11.7 and 9.9%, respectively (Table 2). In relative comparison, MODIS estimates were the highest in March (1.43 mm d^{-1}) and Landsat estimates were highest in December (1.78 mm d^{-1}), as shown in Table 2.

The aggregated 8-km MODIS ET over the Musi catchment was compared with the 8-km AVHRR ET for the period June 2000 to May 2001. The relationships between AVHRR ET and the aggregated MODIS ET for the period are presented as density scatter plots in Fig. 3. As shown in Table 3, the average RMSD was 0.16 mm d^{-1}, ranging from 0.09 to 0.28 mm d^{-1}. The correlation is relatively high (r > 0.75) from September to May but low in June, July, and August (r < 0.59), possibly due to the narrow range of ET values.

The AVHRR ET estimates for the Krishna River Basin from this study were compared with the global ET product of Zhang et al. (2010) (denoted as AVHRR-UMT), which was obtained from the Numerical Terradynamic Simulation Group at the University of Montana (http://ntsg.umt.edu). First, the AVHRR-UMT product was compared with the ET estimates of this study for the lysimeter location in March and December 2000 (see Table 2). The AVHRR-UMT product significantly underestimated ET at the validation site, especially in March, compared with the other estimates of this study. The basin-average annual ET for the period 1983 to2001 was 517 mm yr^{-1} for AVHRR-UMT and 628 mm yr^{-1} for our estimates. This result also indicates overall underestimation by the AVHRR-UMT ET product. The temporal trend of the monthly ET from AVHRR-UMT over the basin is positive at an average rate of 1 mm yr^{-1} yr^{-1}, while our estimates increased at an average rate of 4.97 mm yr^{-1} yr^{-1}. Monthly average ET estimates (1983–2001) are compared in Fig. 4. During Kharif, both estimates were very close, but there was a large difference in the Rabi season (December–May). While both of these products used identical AVHRR NDVI values and surface albedo data, one of the major differences in the input data set was the meteorological data. The AVHRR-UMT product used meteorological data derived from the National Centers for Environmental Prediction–National Center for Atmospheric Research Reanalysis (NNR). The observed difference between the products may have originated from the meteorological inputs based on the comparison with the lysimeter measurements; we can conclude that the use of local meteorological observations improved that accuracy of the ET estimates.

Seasonal Variation of Evapotranspiration

Long-term monthly average ET for the period 1983 to 2001 is plotted in Fig. 5 to present seasonal variations in ET at the basin scale. The peak ET was observed in the Kharif season (June–November), which is due to the monsoon rain and the increased

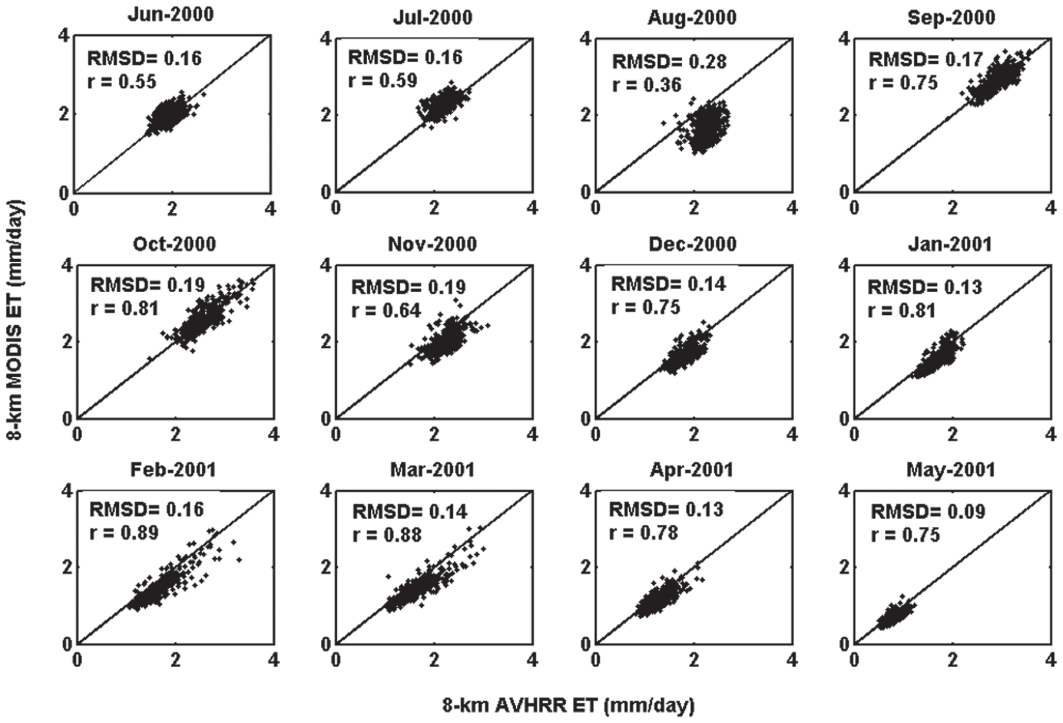

Fig. 3. Comparison of 8-km AVHRR evaporation (ET) (*x* axis) and aggregated 8-km MODIS ET (*y* axis) over the Musi subcatchment (June 2000–May 2001). The lysimeter station is located within this subcatchment.

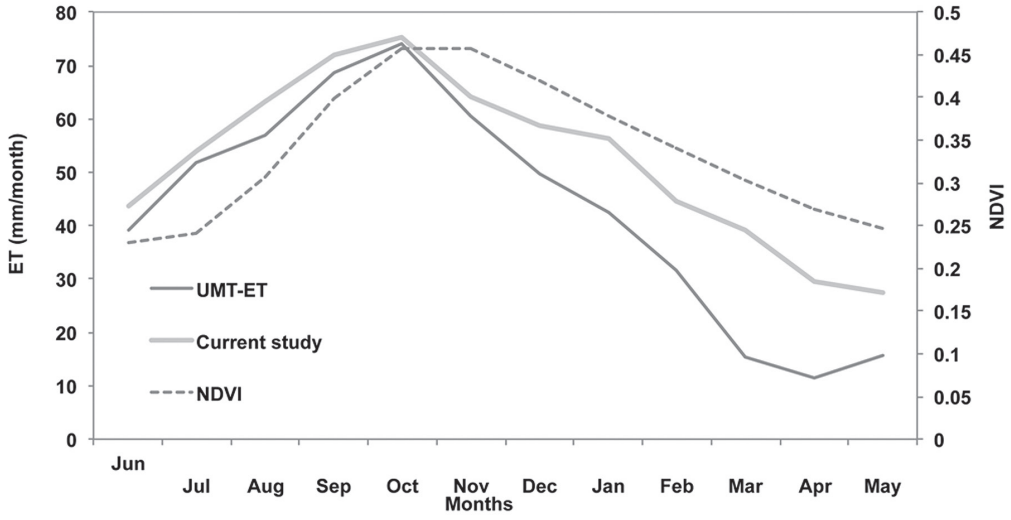

Fig. 4. Comparison of long-term (1983–2011) monthly mean evapotranspiration (ET) estimates from the current study and the AVHRR-UMT ET product over the Krishna River Basin; the normalized difference vegetation index (NDVI) is also shown.

biomass during the Kharif crop-growing season. January and February in the Krishna River Basin is a dry season, however, and relatively high transpiration in the period was estimated (Fig. 5) due to large-scale irrigation for the Rabi (December–March) crops. The average monthly ET was estimated as 61.6 mm mo^{-1} during the Kharif season and 49.5 mm mo^{-1} during the Rabi season.

Long-term basin-scale monthly average ET in Fig. 5 also shows high soil evaporation during monsoon months, increasing from June to August then gradually decreasing. This is due to the high soil water content during the monsoon season. With the start of the Kharif season in June, bare soil evaporation maintains relatively high values due to the wet soil conditions and low canopy cover during

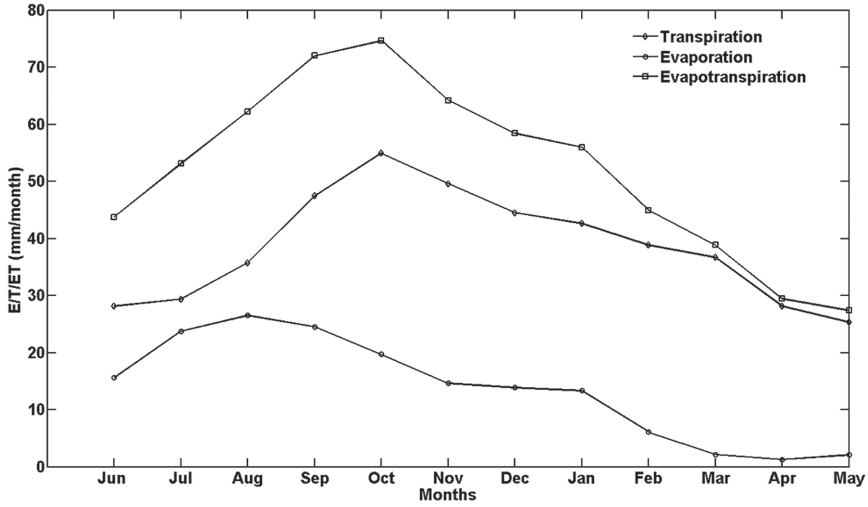

Fig. 5. Long-term (1983–2001) monthly mean of soil evaporation (E), canopy transpiration (T), and total evapotranspiration (ET) over the entire Krishna River Basin.

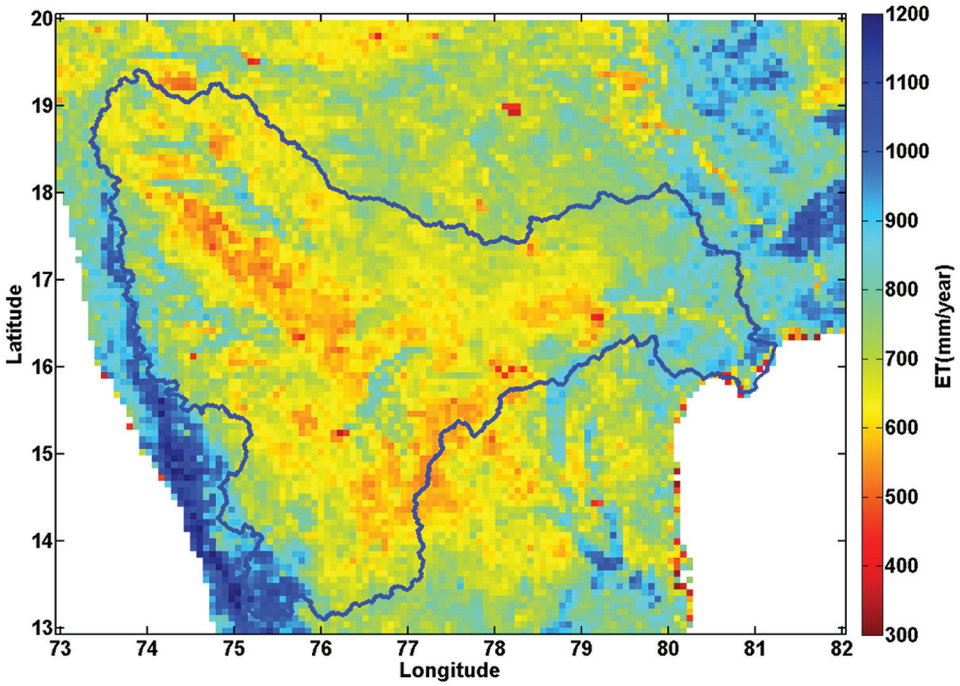

Fig. 6. Spatial distribution of annual evapotranspiration (ET) estimated with 8-km AVHRR data in the Krishna River Basin (June 2000–May 2001).

the early period of crop growth. With time, the vegetation biomass increases and transpiration increases accordingly. Soil evaporation also remains relatively high during the dry season in December and January due to irrigation for the Rabi crops across the downstream region of the basin, as evident from Fig. 5. Except for the Rabi season, seasonal patterns of soil evaporation reflect the monthly rainfall in the basin. The average monthly soil evaporation is estimated as 20.7 mm mo^{-1} in the Kharif season and 8.4 mm mo^{-1} in the Rabi season. Monthly average transpiration estimates show that the vegetation transpiration varies with crop growth, increasing slowly from July to its peak in October, then slowly decreasing (Fig. 5). The average monthly vegetation transpiration was estimated as 40.8 mm mo^{-1} during Kharif and 38.2 mm mo^{-1} during Rabi.

The maps of spatially distributed ET_a (Fig. 6) reflect the spatial patterns of land use. A clear differentiation was observed in the ET patterns, showing wet and highly vegetated classes, such as irrigation service areas and forests, and dry classes, such as dryland

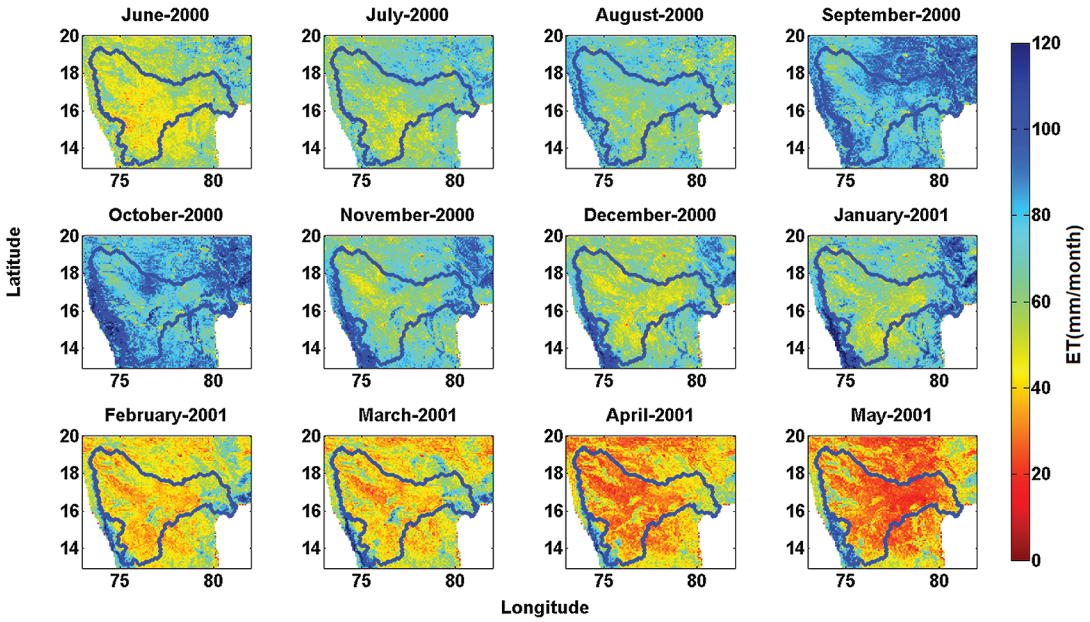

Fig. 7. Monthly evapotranspiration (ET) maps estimated with 8-km AVHRR data from June 2000 to May 2001.

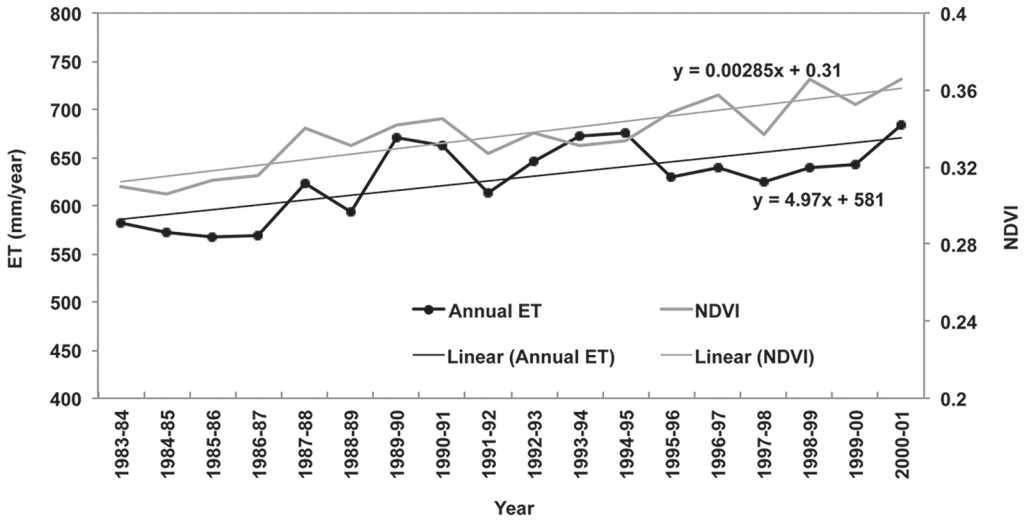

Fig. 8. Interannual variability of the basin-scale normalized difference vegetation index (NDVI) and evapotranspiration (ET) estimated using 8-km AVHRR data over the Krishna River Basin.

and rainfed agriculture during the dry season (March–May). We observed that during the monsoon season, the spatial variation of evapotranspiration was low (see Fig. 7). This is due to the relatively uniform (wet) soil moisture conditions created by the high monsoon rainfall over the whole basin. On the other hand, during dry months, the spatial variation in ET was very high, with only forest and irrigation service areas showing relatively high ET values. The spatial standard deviation of ET during the monsoon season was 10.1 mm mo^{-1}, while it was 13.3 mm mo^{-1} during the dry season. As shown in Fig. 7, the highest ET estimates (>80 mm mo^{-1}) occurred in September and October (peak growth period of Kharif).

Multidecadal Variability and Trends of Evapotranspiration

Annual time series of AVHRR ET estimates over the Krishna River Basin are presented in Fig. 8 to investigate the interannual variability of basin-scale ET for the period 1983 to 2001. The average annual ET during 1983 to 2001 is estimated as 628 mm yr^{-1} and its standard deviation is estimated as 38 mm yr^{-1}. To examine the validity of our results, the AVHRR ET of this study was compared with the ET estimates derived from a simple water balance (ET = precipitation − discharge) of the basin. It showed that the AVHRR ET of this study underestimated the basin-scale

annual ET by 76 mm yr^{-1} on average in 1983 to 2001. Even though the underestimation was significantly smaller than that of the AVHRR-UMT ET (187 mm yr^{-1}), more efforts need to be made to reduce this gap in future research.

A regression analysis of the time series indicated that the annual ET increased continuously at the rate of 4.97 ± 2.73 mm yr^{-1} yr^{-1} (90% confidence interval). No significant changes in annual rainfall (−3.80 mm yr^{-1} yr^{-1}) or solar radiation (−0.88 W m^{-2} yr^{-1} yr^{-1}) were observed during this period. Therefore, this increase in ET was mainly caused by the increase in the irrigated crop area. The basin-scale average NDVI shown in Fig. 8 confirms the increasing trend of overall biomass during the same period. The steeper increase in ET for the period 1983 to 1992 (9.8 mm yr^{-1} yr^{-1}) was due to the rapid expansion of irrigation during the 1980s (see Table 4). After the rapid irrigation development period, the increasing trend was reduced to 2 mm yr^{-1} yr^{-1}.

According to survey data from the Water Resources Department, Government of India, 48 new irrigation projects were commissioned in the Krishna River Basin during the study period. This involved construction of new reservoirs, barrages, and lift irrigation schemes, and the subsequent increase in water storage capacity in existing reservoirs, such as Alamatti, Narayanapur, and Tungabhadra, resulted in expansion of the irrigated area. The total area brought under irrigation during the study period was approximately 1.45 Mha (Table 4). Most of the irrigation development occurred in the upstream part of the basin (MH and KAR).

Table 4. Development of irrigation projects and irrigation area expanded during 1982 to 2001 in the Krishna River Basin by state.

State	Period	Projects completed	Irrigated area expanded	Total irrigated area expanded
		no.	——— ha ———	
Maharashtra	1982–1994	12	371,973	440,478
	1995–2001	5	68,505	
Karnataka	1982–1994	14	684,395	896,046
	1995–2001	7	211,651	
Andhra Pradesh	1982–1994	5	37,504	110,836
	1995–2001	3	73,332	

To examine the impact of irrigation expansion on ET, sub-basin-scale annual ET was analyzed (see Fig. 9). The increasing trend of ET at Upper Bhima (6.5 mm yr^{-1} yr^{-1}) and Middle Krishna (5.2 mm yr^{-1} yr^{-1}) subbasins, where the irrigation expansion was active in the 1980s, was greater than the basin-average increase in ET. On the other hand, the increase in ET in Malaprabha (4.3 mm yr^{-1} yr^{-1}) and Musi (3.3 mm yr^{-1} yr^{-1}) subbasins was smaller

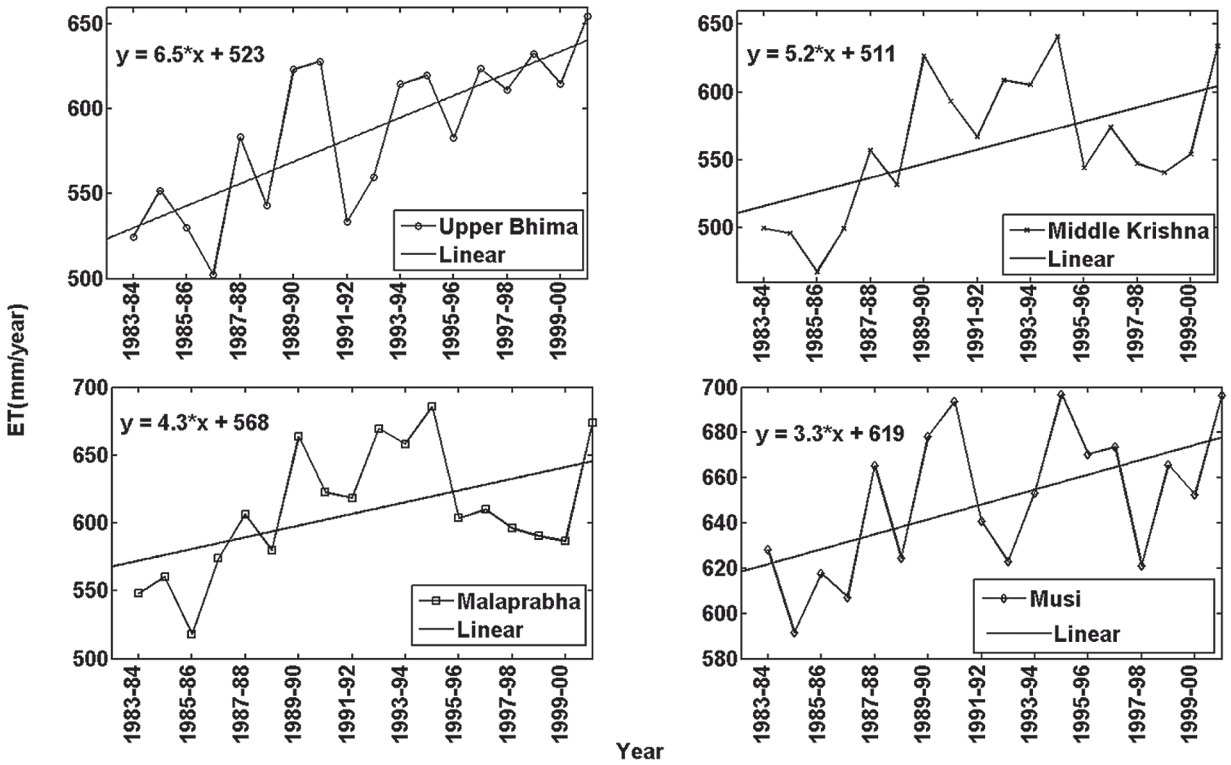

Fig. 9. Time series of annual evapotranspiration (ET) estimates in a selection of subbasins in the Krishna River Basin: (a) Upper Bhima, (b) Middle Krishna, (c) Malaprabha, and (d) Musi.

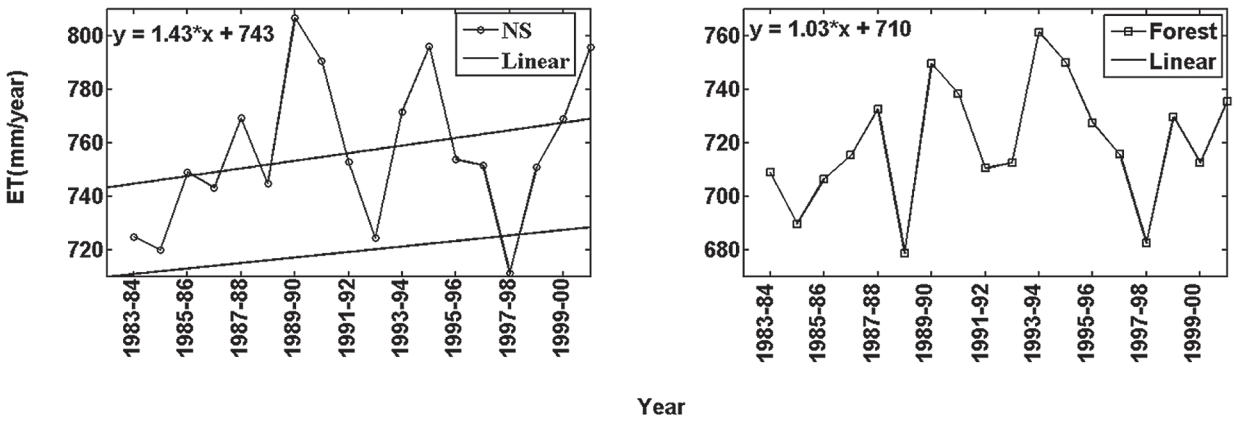

Fig. 10. Time series of annual evapotranspiration (ET) estimates in (a) a preexisting irrigation service area, Nagarjuna Sagar (NS), and (b) a forest region of the Krishna River Basin.

than the basin-average values. This was due to the fact that the irrigation development in Malaprabha and Musi subbasins was completed before our study period. Small-scale groundwater irrigation expanded across these subbasins, however, during the study period (Government of Maharashtra, 2005; Government of Andhra Pradesh, 2006), resulting in a moderate increase in ET.

Interannual variability of ET was also examined in the regions where no significant irrigation development occurred during the study period (Fig. 10). One of the major irrigation service areas, Nagarjuna Sagar (NS), is located in the downstream part of the basin. At NS, irrigation development was completed before the study period, with no significant changes afterward. The NS irrigation service area showed an annual increase of 1.45 mm yr^{-1} yr^{-1}, which is much lower that the basin average. The Krishna Delta, another irrigation service area where development was completed before the study period, also showed a trend similar to that of the NS service area (1.84 mm yr^{-1} yr^{-1}). In addition, we analyzed changes in ET in the Srisailam forest located in the downstream part of the basin. It showed only 1 mm yr^{-1} yr^{-1} increase (Fig. 10) during the study period. This confirms that the irrigation expansion made a significant contribution to the observed increasing trend in the basin-average ET.

The steep increase in ET due to irrigation development is also evidenced by the trend in biomass represented by the NDVI. During the study period, the average increasing rate of NDVI in the Upper Bhima service area (0.0041 yr^{-1}) was approximately five times larger than that in the NS irrigation service area (0.0008 yr^{-1}).

Summary and Conclusions

Historical basin-scale ET was calculated using the GIMMS AVHRR satellite data and daily local meteorological data for the Krishna River Basin. Monthly time series of ET maps was prepared using a modified PM approach, with biome-specific canopy conductance determined from NDVI. Validation included field-scale comparison between 30-m Landsat ET and the lysimeter measurement, which exhibited a mean difference of 5.3%. The validated Landsat ET was subsequently used to validate 250-m MODIS ET and then finally to validate 8-km AVHRR ET estimates for 2000 to 2001. The AVHRR-derived ET estimates of this study had an error <14% when compared with the Landsat-derived ET estimates.

The AVHRR ET estimates of this study showed that the basin-average ET increased at the rate of 4.97 mm yr^{-1} yr^{-1} in the Krishna River Basin during the period 1983 to 2001. No significant trends in rainfall or solar radiation were observed during the period. Sub-basin-scale analyses of ET showed that the expansion of irrigated area during the study period was probably responsible for the observed increase in ET in the basin. The irrigation service areas developed in the 1980s showed significantly higher increasing trends in ET than the preexisting irrigation service area and the forest.

Acknowledgments

The research is funded by the Australian Centre for International Agricultural Research (ACIAR) under the John Allwright Fellowship and ACIAR Project LWR-2007-113. We would like to thank the Indian Meteorological Department (IMD), International Water Management Institute (IWMI), International Crops Research Institute for the Semi-Arid Tropics (ICRISAT), Central Research Institute for Dryland Agriculture (CRIDA), and the Indian Institute of Tropical Meteorology (IITM) for providing daily meteorological and other ancillary data.

References

Allen, R.G., L.A. Pereira, D. Raes, and M. Smith. 1998. Crop evapotranspiration guidelines for computing crop water requirements. FAO Irrig. Drain. Pap. 56. FAO, Rome.

Allen, R.G., M. Tasumi, A. Morse, R. Trezza, J. Wright, W. Bastiaanssen, et al. 2007a. Satellite-based energy balance for Mapping Evapotranspiration with Internalized Calibration (METRIC) applications. J. Irrig. Drain. Eng. 133:395–406. doi:10.1061/(ASCE)0733-9437(2007)133:4(395)

Allen, R.G., M. Tasumi, and R. Trezza. 2007b. Satellite-based energy balance for Mapping Evapotranspiration with Internalized Calibration (METRIC) model. J. Irrig. Drain. Eng. 133:380–394. doi:10.1061/(ASCE)0733-9437(2007)133:4(380)

Australian National Water Commission. 2007. Australian water resources 2005: Evapotranspiration. NWC, Canberra, ACT. http://www.water.gov.au/WaterAvailability/Whatisourtotalwaterresource/Evapotranspiration/index.aspx?Menu=Level1_3_1_4.

Bastiaanssen, W.G.M., M. Menenti, R.A. Feddes, and A.A.M. Holtslag. 1998a. A remote sensing surface energy balance algorithm for land (SEBAL): I. Formulation. J. Hydrol. 212–213:198–212. doi:10.1016/S0022-1694(98)00253-4

Bastiaanssen, W.G.M., H. Pelgrum, J. Wang, Y. Ma, J.F. Moreno, G.J. Roerink, and T. van der Wal. 1998b. A remote sensing surface energy balance algorithm for land (SEBAL): II. Validation. J. Hydrol. 212–213:213–229. doi:10.1016/S0022-1694(98)00254-6

Biggs, T.W., A. Gaur, C.A. Scott, P. Thenkabail, P. GangadharaRao, M.K. Gumma, et al. 2007. Closing of the Krishna basin: Irrigation, streamflow depletion, and macroscale hydrology. IWMI Res. Rep. 111. Int. Water Manage. Inst., Colombo, Sri Lanka.

Biggs, T.W., P.K. Mishra, and H. Turral. 2008. Evapotranspiration and regional probabilities of soil moisture stress in rainfed crops, southern India. Agric. For. Meteorol. 148:1585–1597. doi:10.1016/j.agrformet.2008.05.012

Bouchet, R.J. 1963. Evapotranspiration réelle evapotranspiration potentielle, signification climatique. In: Committee for Evaporation, General Assembly of Berkeley. 19–31 Aug. 1963. IAHS Publ. 62. Int. Assoc. Hydrol Sci., Wallingford, UK. p. 132–142.

Bouwer, L.M., J.C.J.H. Aerts, P. Droogers, and A.J. Dolman. 2006. Detecting the long-term impacts from climate variability and increasing water consumption on runoff in the Krishna River Basin (India). Hydrol. Earth Syst. Sci. 10:703–713. doi:10.5194/hess-10-703-2006

Cleugh, H.A., R. Leuning, Q. Mu, and S.W. Running. 2007. Regional evaporation estimates from flux tower and MODIS satellite data. Remote Sens. Environ. 106:285–304. doi:10.1016/j.rse.2006.07.007

DehghaniSanij, H., T. Yamamoto, and V. Rasiah. 2004. Assessment of evapotranspiration estimation models for use in semi-arid environments. Agric. Water Manage. 64:91–106. doi:10.1016/S0378-3774(03)00200-2

Dingman, S.L. 2008. Physical hydrology. 2nd ed. Prentice Hall, Upper Saddle River, NJ.

Drexler, J.Z., R.L. Snyder, D. Spano, and K.T. Paw U. 2004. A review of models and micrometeorological methods used to estimate wetland evapotranspiration. Hydrol. Processes 18:2071–2101. doi:10.1002/hyp.1462

Ferguson, C.R., J. Sheffield, E.F. Wood, and H. Gao. 2010. Quantifying uncertainty in a remote sensing-based estimate of evapotranspiration over continental USA. Int. J. Remote Sens. 31:3821–3865. doi:10.1080/01431161.2010.483490

Fisher, J.B., K.P. Tu, and D.D. Baldocchi. 2008. Global estimates of the land–atmosphere water flux based on monthly AVHRR and ISLSCP-II data, validated at 16 FLUXNET sites. Remote Sens. Environ. 112:901–919.

George, B., H. Malano, B. Davidson, P. Hellegers, L. Bharati, and S. Massuel. 2011. An integrated hydro-economic modelling framework to evaluate water allocation strategies: I. Model development. Agric. Water Manage. 98:733–746. doi:10.1016/j.agwat.2010.12.004

Government of Andhra Pradesh. 2006. Minor irrigation census statistics. Directorate of Economics and Statistics, HYderabad, AP, India.

Government of Maharashtra. 2005. Minor irrigation census statistics. Ministry of Water Resources, Mumbai, MH, India.

Gowda, P.H., J.L. Chavez, P.D. Colaizzi, S.R. Evett, T.A. Howell and J.A. Tolk. 2008. ET mapping for agricultural water management: Present status and challenges. Irrig. Sci. 26:223–237. doi:10.1007/s00271-007-0088-6

Haddeland, I., D.P. Lettenmaier, and T. Skaugen. 2006. Effects of irrigation on the water and energy balances of the Colorado and Mekong river basins. J. Hydrol. 324:210–223. doi:10.1016/j.jhydrol.2005.09.028

Jackson, R.B., S.R. Carpenter, C.N. Dahm, D.M. McKnight, R.J. Naiman, S.L. Postel, and S.W. Running. 2001. Water in a changing world. Ecol. Appl. 11:1027–1045. doi:10.1890/1051-0761(2001)011[1027:WIACW]2.0.CO;2

Kalma, J.D., T.R. McVicar, and M.F. McCabe. 2008. Estimating land surface evaporation: A review of methods using remotely sensed surface temperature data. Surv. Geophys. 29:421–469. doi:10.1007/s10712-008-9037-z

Kustas, W.P., F. Li, T.J. Jackson, J.H. Prueger, J.I. MacPherson, and M. Wolde. 2004. Effects of remote sensing pixel resolution on modeled energy flux variability of croplands in Iowa. Remote Sens. Environ. 92:535–547. doi:10.1016/j.rse.2004.02.020

Kustas, W.P., J.M. Norman, M.C. Anderson, and A.N. French 2003. Estimating subpixel surface temperatures and energy fluxes from the vegetation index–radiometric temperature relationship. Remote Sens. Environ. 85:429–440. doi:10.1016/S0034-4257(03)00036-1

Leuning, R., Y.Q. Zhang, A. Rajaud, H. Cleugh, and K. Tu. 2008. A simple surface conductance model to estimate regional evaporation using MODIS leaf area index and the Penman–Monteith equation. Water Resour. Res. 44:W10419. doi:10.1029/2007WR006562

Li, F., W.P. Kustas, M.C. Anderson, J.H. Prueger, and R.L. Scott. 2008. Effect of remote sensing spatial resolution on interpreting tower-based flux observations. Remote Sens. Environ. 112:337–349. doi:10.1016/j.rse.2006.11.032

Mohan, S., and N. Arumugam. 1994. Crop coefficients of major crops in South India. Agric. Water Manage. 26:67–80. doi:10.1016/0378-3774(94)90025-6

Monteith, J.L. 1965. Evaporation and the environment. In: The state and movement of water in living organisms:19tht Symposium of the Society for Experimental Biology, Swansea. Cambridge Univ. Press, Cambridge, UK. p. 205–234.

Mu, Q., F.A. Heinsch, M. Zhao, and S.W. Running. 2007. Development of a global evapotranspiration algorithm based on MODIS and global meteorology data. Remote Sens. Environ. 111:519–536. doi:10.1016/j.rse.2007.04.015

Paco, T.A., M.I. Ferreira, and N. Conceicao. 2006. Peach orchard evapotranspiration in a sandy soil: Comparison between eddy covariance measurements and estimates by the FAO 56 approach. Agric. Water Manage. 85:305–313. doi:10.1016/j.agwat.2006.05.014

Pinker, R.T., and I. Laszlo. 1992. Modeling surface solar irradiance for satellite applications on a global scale. J. Appl. Meteorol. 31:194–211. doi:10.1175/1520-0450(1992)031<0194:MSSIFS>2.0.CO;2

Priestley, C.H.B., and R.J. Taylor. 1972. On the assessment of surface heat flux and evaporation using large-scale parameters. Mon. Weather Rev. 100:81–92. doi:10.1175/1520-0493(1972)100<0081:OTAOSH>2.3.CO;2

Su, Z. 2002. The Surface Energy Balance System (SEBS) for estimation of turbulent heat fluxes. Hydrol. Earth Syst. Sci. 6:85–99. doi:10.5194/hess-6-85-2002

Tasumi, M., R. Allen, R.G. Trezza, and J.L. Wright. 2005. Satellite-based energy balance to assess within-population variance of crop coefficient curves. J. Irrig. Drain. Eng. 131:94–109. doi:10.1061/(ASCE)0733-9437(2005)131:1(94)

Thenkabail, P. S., C. M. Biradar, P. Noojipady, V. Dheeravath, Y. Li, M. Velpuri, et al. 2009. Global irrigated area map (GIAM), derived from remote sensing, for the end of the last millennium. Int. J. Remote Sens. 30:3679–3733. doi:10.1080/01431160802698919

Thenkabail, P.S., P. GangadharaRao, T.W. Biggs, M. Krishna, and H. Turral. 2007. Spectral matching techniques to determine historical land use/land cover (LULC) and irrigated areas using time-series AVHRR Pathfinder datasets. Photogramm. Eng. Remote Sens. 73:1029–1040.

Tucker, C.J., J.E. Pinzon, M.E. Brown, D.A. Slayback, E.W. Pak, R. Mahoney, et al. 2005. An extended AVHRR 8 km NDVI data set compatible with MODIS and SPOT vegetation NDVI data. Int. J. Remote Sens. 26:4485–4498. doi:10.1080/01431160500168686

Tyagi, N.K., D.K. Sharma, and S.K. Luthra. 2000. Determination of evapotranspiration and crop coefficients of rice and sunflower with lysimeter. Agric. Water Manage. 45:41–54. doi:10.1016/S0378-3774(99)00071-2

Van Rooijen, D.J., T.W. Biggs, I. Smout, and P. Drechel. 2010. Urban growth, wastewater production and use in irrigated agriculture: A comparative study of Accra, Addis Ababa and Hyderabad. Irrig. Drain. Syst. 24:53–64. doi:10.1007/s10795-009-9089-3

Venot, J.-P., H. Turral, M. Samad, and F. Molle. 2007. Shifting waterscapes: Explaining basin closure in the Lower Krishna Basin, South India. IWMI Res. Rep. 121. Int. Water Manage, Inst., Colombo, Sri Lanka.

Vinukollu, R.K., R. Meynadier, J. Sheffield, and E.F. Wood. 2011a. Multi-model, multi-sensor estimates of global evapotranspiration: Climatology, uncertainties and trends. Hydrol. Processes 25:3993–4010. doi:10.1002/hyp.8393

Vinukollu, R.K., E.F. Wood, C.R. Ferguson, and J.B. Fisher. 2011b. Global estimates of evapotranspiration for climate studies using multi-sensor remote sensing data: Evaluation of three process-based approaches. Remote Sens. Environ. 115:801–823. doi:10.1016/j.rse.2010.11.006

Wilcox, B.P., D.D. Breshears, and M.S. Seyfried. 2003. Water balance on rangelands. In: B.A. Stewart and T.A. Howell, editors, Encyclopedia of Water Science. Marcel Dekker, New York. p. 791–794.

Zhang, K., J.S. Kimball, Q. Mu, L.A. Jones, S.J. Goetz, and S.W. Running. 2009. Satellite based analysis of northern ET trends and associated changes in the regional water balance from 1983 to 2005. J. Hydrol. 379:92–110. doi:10.1016/j.jhydrol.2009.09.047

Zhang, K., J.S. Kimball, R.R. Nemani, and S.W. Running. 2010. A continuous satellite-derived global record of land surface evapotranspiration from 1983 to 2006. Water Resour. Res. 46:W09522. doi:10.1029/2009WR008800